Taylor & Francis
Taylor & Francis Group

Corrosion Engineering, Science and Technology

The International Journal of Corrosion Processes and Corrosion Control

ISSN: 1478-422X (Print) 1743-2782 (Online) Journal homepage: https://www.tandfonline.com/loi/ycst20

# Synthesis and high-temperature corrosion resistance of Ti-Zr-Si-N coatings deposited by means of sputtering

Julieta Cardenas, Jersson Leon & Jhon J. Olaya

**To cite this article:** Julieta Cardenas, Jersson Leon & Jhon J. Olaya (2019): Synthesis and high-temperature corrosion resistance of Ti-Zr-Si-N coatings deposited by means of sputtering, Corrosion Engineering, Science and Technology, DOI: 10.1080/1478422X.2019.1573498

**To link to this article:** https://doi.org/10.1080/1478422X.2019.1573498

Published online: 31 Jan 2019.

CORROSION ENGINEERING, SCIENCE AND TECHNOLOGY
https://doi.org/10.1080/1478422X.2019.1573498

The Institute of Materials, Minerals and Mining

Taylor & Francis
Taylor & Francis Group



# Synthesis and high-temperature corrosion resistance of Ti-Zr-Si-N coatings deposited by means of sputtering

Julieta Cardenas [a,b], Jersson Leon [a,b] and Jhon J. Olaya [a]

[a]Department of Mechanical and Mechatronic Engineering, Universidad Nacional de Colombia Sede Bogotá, Bogotá, Colombia; [b]School of Electromechanical Engineering, Universidad Pedagógica y Tecnológica de Colombia, Duitama, Colombia

**ABSTRACT**

We present a study of the synthesis and an evaluation of the corrosion resistance of Ti-Zr-Si-N coatings deposited by means of the co-sputtering technique on 316L steel and Ti6Al4V alloy substrates. The thin films were obtained using $Ti_5Si_2$ and Zr targets with 99.9% purity for the deposition, and a power of 200 W was applied in the DC source and 170 W in the RF source. The corrosion resistance was evaluated via the cyclic oxidation test with consistent cycles of 1 hour of cooling, 1 hour of heating, and 16 minutes of stabilisation for 300 cycles at a temperature of 600°. The coatings were characterised by means of scanning electron microscopy (SEM), X-ray diffraction (XRD), and confocal laser microscopy. The coating was effective up to 150 cycles for the case of 316L steel, and up to 50 cycles for the Ti6AlV alloy.

**ARTICLE HISTORY**
Received 19 September 2018
Revised 26 December 2018
Accepted 19 January 2019

**KEYWORDS**
Ti-Zr-Si-N coatings; co-sputtering; corrosion resistance

## Introduction

In recent years, there has been great interest in the investigation of a new generation of nanostructured coatings [1] consisting of at least two phases, with nanocrystalline and/or amorphous structures. These materials possess unique physical and functional properties and are widely used as diffusion barriers, wear resistant coatings on cutting tools, and corrosion and abrasion resistant layers on optical and mechanical components. Among these materials, composite coatings with TiN and ZrN stand out, which when combined produce a material with high resistance to corrosion and wear, with a golden hue [2].

The characteristics of TiN in the form of thin films have been widely studied, due to its excellent resistance to wear, its hardness, and its optical and chemical properties [3]. The presence of covalent, ionic, and metallic bonds confer the characteristics of ceramics (hardness) and the properties of metal alloys, hence its main use as a diffusion barrier in gate electrodes in metal-oxide field-effect transistors (MOFET), optical coatings in solar cells, and protective layers [4,5]. On the other hand, ZrN is a protective transmetallic-type nitride compound that exhibits excellent chemical stability. Currently, research has focused on the study of this material as a reflective coating, because of its optical properties. This material has applications in mechanical components such as wear-resistant hard coatings [6]. Multicomponent alloy systems, comprising more than three elements with different atomic concentrations, have complex microstructures that include a solid solution, amorphous phases, and/or intermetallic compounds [7].

However, (Ti, Zr) N coatings exhibit improved hardness compared to coatings of TiN or ZrN deposited under the same conditions [8,9,10]. Studies of this compound indicate good adhesion and high hardness, due to a solid solution strengthening mechanism that provides an energetic barrier for the movement of the dislocations through the crystals through the distortion in the network parameter [11]. The addition of Si into transitional nitrides produces nanocomposites by forming nanocrystals of TiN and ZrN embedded in the formation of an amorphous phase of silicon nitride. The improved properties of the Zr-Ti-Si-N system have been attributed to the refinement of the grain size, in which one or more phases are present at the nanoscale to form a nanocomposite. It is also believed that the formation of amorphous SiNx interlayers at the grain boundaries suppresses the oxidation process along these highly diffusive pathways, thus protecting the surrounding TiN/SiNx structure. Therefore, the addition of Si into (Ti, Zr) N films is beneficial in terms of hardness, resistance to corrosion, and improvement of the stability of the radiation [12,13].

The aim of the present research was to synthesise Ti-Zr-Si-N films by means of the co-sputtering technique and evaluate the corrosion resistance through cyclic oxidation on 316L stainless steel and Ti6Al4V alloy substrates. We performed chemical composition measurements and characterised the microstructure in order to understand the structural changes in the coatings during the oxidation tests.

## Experimental

### Material and solutions

The coatings were deposited with a co-sputtering system, illustrated in Figure 1. Two targets with 99.9% purity were used to generate the plasma. The discharge was done with a power of 170 W for the $Ti_5Si_2$ target and 200 W for the Zr target. In the first phase of the synthesis, the coatings were produced by varying the deposition temperature and the discharge power, selecting for this study the coating with the highest adhesion. Table 1 summarises the main parameters of the discharge for the manufacture of the coatings.

In this investigation, rectangular AISI SAE 316L steel substrate samples of $1.7 \times 1.5 \times 0.3$ cm and cylindrical Ti6Al4V alloy substrate samples of 16 mm in diameter and 3 mm in thickness were used. These substrates were polished with

CONTACT Jhon J. Olaya jjolayaf@unal.edu.co

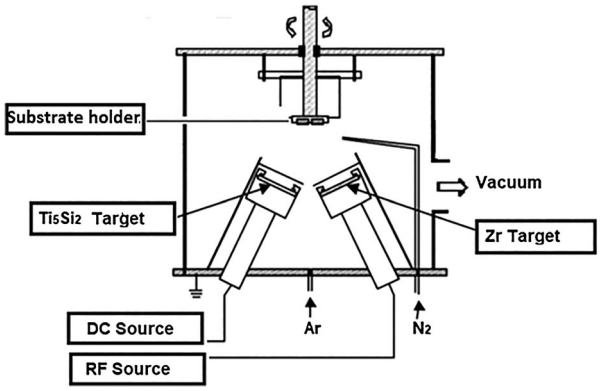


**Figure 1.** Schematic representation of the co-sputtering system.

silicon carbide abrasive paper up to a grain of 2500, and then in order to achieve a mirror finish, a 1 $u$m alumina solution ($Al_2O_3$) impregnated into a cloth was used. The final cleaning of the samples in Branson 1510R-DTH ultrasound equipment was initially performed with acetone and then with isopropanol for five minutes each.

The X-ray diffraction analysis (XRD) was performed on X'pert Pro Panalytical equipment, with data taken at an angle of 2θ between 10° and 120°, using an RTMS (real-time multiple strip) detector with Cu Kα radiation at a wavelength of 1542 Å and a step size of 0.0263° in Bragg-Brentano mode, before and after the cyclic oxidation test, in order to determine the phases present. In order to determine crystalline changes as a function of temperature, complementary XRD measurements were made as a function of the temperature up to 1100°C.

The morphological analysis was performed with a FEI QUANTA 200 scanning electron microscope in secondary electron mode in a high vacuum with a voltage of 30 KV. The qualitative chemical composition analysis was done by means of an EDS energy-dispersion microprobe. The study of the change in roughness was characterised using a Zeiss LSM700 Zen 2009 confocal laser microscope with a 405 µm high-pass laser and a cutoff of Λc = 250.

The thickness measurement was done on a DEKTAK 150 profilometer with 1500 µm sweep in the ridges and valleys with duration of 60 s, applying a force of 2.50 g and a resolution of 0.056 µm per sample. The deposition time was one hour, in order to achieve a thickness of approximately 800 nm.

The corrosion test was carried out in an inverted cyclic test furnace, in an air environment without gas flow, with a temperature of 600°C, where each cycle consisted of a heating stage and a cooling stage. The duration was 60 min for each of these stages, with 16 min of stabilisation, in order to reach the temperature, as shown in Figure 2.

**Table 1.** Deposition parameters used in the discharge.

| Deposition parameters | |
|---|---|
| Base pressure (mbar) | $9.5 \times 10^{-6}$ |
| Work pressure (mbar) | $4.0 \times 10^{-3}$ |
| Gas flow (sccm) | Ar:14$N_2$:2 |
| Time (min) | 60 |
| DC power (W) | 200 |
| Target-substrate distance (cm) | 10.16 |
| RF power (W) | 170 |
| Temperature (°C) | 260 |
| Rotation of substrate carrier (rev $min^{-1}$) | 10 |

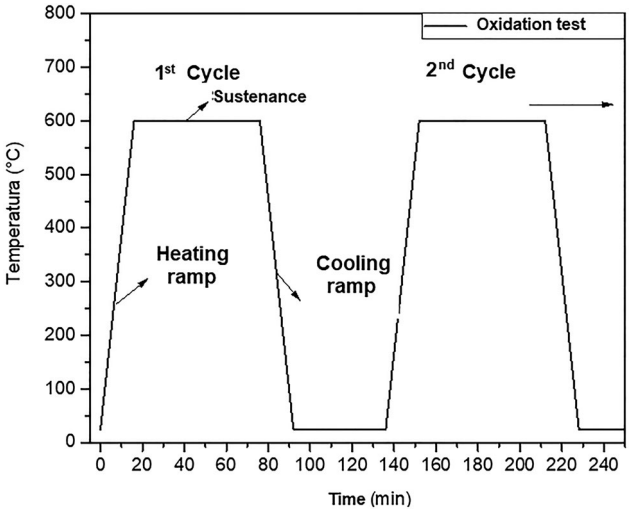


**Figure 2.** Cyclic oxidation test.

The total number of cycles for the tests was 300, taking samples in order to analyse the variation in mass of both the substrate and the coating at cycles 0, 5, 10, 25, 35, 50, 100, 150, 200, and 300. Mass loss was measured with a Cole-Parmer Symmetry digital scale with an accuracy of 0.0001 gr. The measurement of the variations in the mass analysed for the two substrates with and without coating was carried out according to the method proposed by the ASTM G1 standard.

## Results and discussion

### *Characterisation of the coatings*

Figure 3(a) shows the XRD analysis of Ti-Zr-Si-N coatings deposited on 316L steel substrates. Peaks can be seen at positions 2 θ 35.125° 39.954°, 58.975°, and 75.215°, with the crystallographic planes (111), (200), (220), and (222), respectively, corresponding to the formation of the solid solution (Ti, Zr) N, which agrees with other investigations [14–16]. Figure 3(b) shows the XRD analysis of the Ti-Zr-Si-N coatings deposited on the Ti6Al4V alloy. Here, peaks can also be seen at positions 2 θ 35.125° 39.954°, 58.975°, and 75.215°, with the crystallographic planes described for 316L steel, which corroborates the formation of the solid solution (Ti, Zr) N with a strong (111) orientation.

The other peaks shown in the figures correspond to signals of the substrate. The X-ray diffraction pattern did not show $Si_3N_4$ peaks, which indicates its amorphous nature [17]; however, the incorporation of silicon into the ZrN- and Ti-based coatings is important, because it can increase the hardness, improve the resistance to oxidation, and reduce the coefficient of friction of the films [18]. Amorphous coatings such as $a$-$Si_3N_4$ exhibit high corrosion resistance due to their dielectric nature and dense microstructure without preferential corrosion routes such as grain boundaries and other structural defects [19,20].

Table 2 shows the EDS spectrometry analysis with the percentages of atomic concentration. The results indicate the presence of elements of the substrate such as Fe, Cr, and Ni for the coating deposited on 316L steel. Furthermore, the presence of Ti, Zr, Si, and N in the coating is evident. With these results, it can be seen that the zirconium obtained the

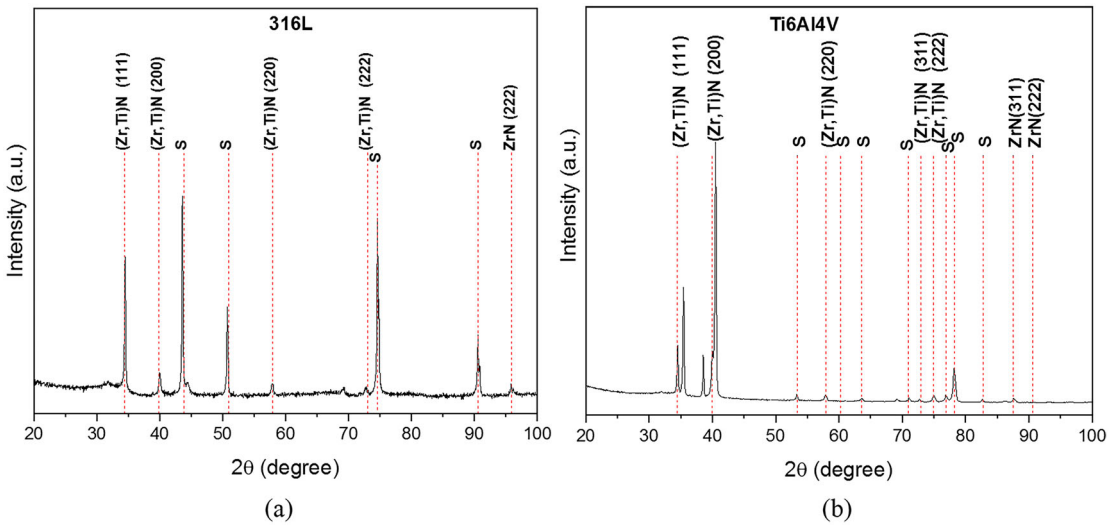


**Figure 3.** X-ray diffractogram of Ti-Zr-Si-N coating deposited on (a) 316L steel substrate and (b) Ti6Al4V substrate

highest percentage of atomic concentration, with 28.42%, the titanium was in the range of 3.08%, and silicon was at 2.84%, whereas the EDS analysis for the coating-Ti6Al4V alloy system shows the presence of aluminium, titanium, and vanadium from the substrate, as well as the presence of the coating (Ti-Zr-Si-N). In this analysis, titanium exhibited the highest value, with 73.04%, followed by zirconium and silicon with 2.09% and 1.07%, respectively.

Table 3 shows the crystallite size and the microdeformation of the coatings deposited on both substrates, which was determined using the Williamson-Hall method and the Debye–Scherrer equation [20]. It can be seen that for the (111) and (200) planes, the size varies between 18 and 23 nm for the coating deposited on 316Lsteel, while the size for the Ti-Zr-Si-N coating deposited on the Ti6Al4V alloy varies between 22 and 24 nm.

Figure 4 shows the micrographs of a cross-section of the Ti-Zr-Si-N coating deposited on the silicon substrate, where a thin film layer with compaction and few microstructural voids is clearly evident. In general, a compact, smooth, and homogeneous structure can be seen, without cracks and without delamination of the coating. According to the microstructure shown, it can be inferred that it is columnar, with a structural zone T where the formation of the film begins with the development of very small grains, where surface diffusion makes possible the migration of atoms between adjacent grains [20].

Figure 5(a) shows the X-ray diffraction patterns of the coating deposited on 316Lsteel heated up to 500°C, and in Figure 5(b), the results achieved are shown up to 1100°C, taking diffractograms every 100°C. The results show the peaks of the coating (Zr, Si, Ti)N up to 500°C, with a decrease in their intensity; however, with the increase in temperature, the peaks that correspond to the coating disappear, and above 600°C, the beginning of the formation of oxidation products can be seen. Spikes of oxide of the coating are indexed as $ZrO_2$ in the planes (101) and (200), which are in positions 2θ 29.869° and 50.06°, respectively, and which correspond to the tetragonal phase of $ZrO_2$, $TiO_2$ in planes (100), (110), (200), and (112) at positions 34.14°, 61.72°, 71.35°, and 88.63° (PDF 01-085-2084), and $SiO_2$ at peaks 35.65°, 40.11°, and 48.81° (PDF 013 -0026) with planes (113), (222), and (303), respectively. Some oxides can also be seen with elements of the substrate such as $Fe_2O_3$ (PDF01-088-2359) and CrO, with peaks at2θ 43.7°, 74.4°, and 90.7° (PDF 006-0532) in planes (400), (533), and (731), respectively. Table 4 shows the oxides formed from the diffraction pattern shown in Figure 5(b) as the temperature increased.

**Table 2.** EDS concentration for the coating deposited on 316L steel and Ti6Al4V alloy.

| 316L | | Ti6Al4V | |
|---|---|---|---|
| Element | Atomic composition (at.-%) | Element | Atomic composition (at.-%) |
| Fe K | 46.62 | Ti K | 73.07 |
| Cr K | 13.25 | Al K | 14.19 |
| Ni K | 5.76 | N K | 4.17 |
| Si K | 2.84 | V K | 3.88 |
| TiK | 3.08 | Zr K | 2.09 |
| ZrK | 28.42 | Si K | 1.07 |
| Fe K | 46.62 | | |

## *Cyclic oxidation test*

Figure 6 shows the behaviour of the mass variation during the 300 cycles applied during the tests at a temperature of 600°C for the 316Lsteel and Ti6Al4V alloy substrates with coating. These results were adjusted by means of regressions in order to approximate the behaviour of the kinetics of corrosion undergone by each substrate with a Ti-Zr-Si-N coating. In general, it can be seen that the variation in mass increases for each cycle of the test. In the first cycles of the experiment, the oxidation behaviour of the coatings was exponential, where the coating was in contact with air, and later at a high temperature it produced a layer of oxides that were slowly generated [21,22]. Figure 6(b) shows the behaviour of the variation in mass during 300 cycles for the Ti6Al4V alloy. As shown in the graph, the generation of oxide layers was constant, which is associated with the movement of metal cations during the stage of oxide growth towards the outside, which generates voids that separate the

**Table 3.** Crystallite size of Ti-Zr-Si-N coating.

| Substrate | Plane | Peak (2θ) | Crystallite size (nm) | E |
|---|---|---|---|---|
| 316L | (111) | 35.021 | 23.37 | 3.69 |
| | (200) | 39.99 | 18.14 | 3.16 |
| Ti6Al4V | (111) | 35.37 | 24.54 | 3.75 |
| | (200) | 39.78 | 22.14 | 3.71 |

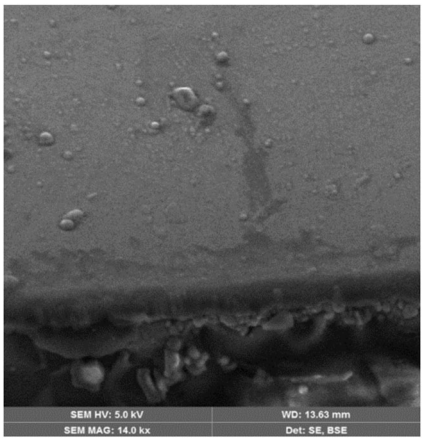


**Figure 4.** SEM micrographs of a cross-section of the microstructure of the Ti-Zr-Si-N film.

oxide layer and the Ti6Al4V substrate [23–25]. It can be seen that the change in mass becomes greater as the number of thermal corrosion cycles increases, which indicates that the oxide layer has a certain protective behaviour [21,26].

Figure 7 shows the topography of the coating subjected to oxidation for 100, 200, and 300 cycles, respectively. The analysis was carried out by means of confocal laser microscopy and indicates that the surface of the Ti-Zr-Si-N coatings deposited with a subsequent cyclic oxidation test is not homogeneous. These images show a rough surface of the coatings, where regions appear that are related to corrosion products. The generated products could be associated with layers of rough oxides of opaque colour and with the presence of specific defects, products of the mechanism of diffusion of iron cations from the substrate towards the outside.

Figure 8 shows the average roughness values for the coating analysed in cycles 10, 25, 50, 100, 200, and 300. The value of Ra varies between 0.786 and 1.994 and Rsa between 0.889 and 2.655 for the coating deposited on 316L steel. The value of Ra is between 0.682 and 4.57, with Rsa between 0.709 and 10.09 for the coating deposited on Ti6Al4V alloy. The roughness in the coatings obtained after the cyclic oxidation test indicates that it is higher for the TiA6l4V substrate, possibly due to the amount of oxide layers formed on the surface.

Figure 9 shows the SEM analysis for the coated substrate subjected to cyclic oxidation, in parts (a), (b), and (c) for

**Table 4.** Oxides formed according to the XRD pattern in Figure 5.

| Phase | 2θ | Phase | 2θ | Phase | 2θ |
|---|---|---|---|---|---|
| $ZrO_2$ | 29.978 | $TiO_2$ | 23.905 | $FeTiO_3$ | 63.157 |
| | 61.721 | | 32.83 | | 87.195 |
| | 71.353 | | 40.437 | CrO | 43.7 |
| | 73.0897 | | 42.735 | | 74.4 |
| | 83.777 | | 56.827 | | 90.7 |
| | 88.511 | | | | |
| | 94.27 | | | | |

316L steel. The composition of the defects of the coating-stainless steel system is made up of compounds formed by Fe, Cr, and O, determined by EDS (not shown). The generation of larger cores of corrosion products and the presence of larger defects become visible, where the formation of compound-type metal oxides of chromium and iron can be seen, belonging to the substrate. Some corrosion products could be associated with the grain boundaries of the 316L steel, due to sensitisation phenomena that occur in stainless steels at high temperatures. In this system, there was a localised attack where the cracks formed, generating the exposure of the substrate after the 150 cycles. These results were corroborated via SEM/EDS analysis, where after the specified cycles there was no evidence of the coating, but only of the oxides formed as the test progressed. In the coating-Ti6Al4V system (Figure 9 (d–f)), the formation of oxides can be seen as layers mainly formed by ruil and anastase. The generation of an inhomogeneous layer of corrosion products is evident, as well as the generation of isolated nuclei of pore-type defects. However, by means of SEM it was determined that after the 50 cycles huge iron oxide layers were generated, due to the attack produced, reaching the surface of the substrate and causing delamination of the coating.

In general, the SEM analyses show the appearance of defects such as cracks and pores due to thermal shock and to the difference between the coefficients of thermal expansion of the coating and the substrate, as well as the presence of corrosion products located preferentially on the voids [21].

Figure 10 shows the cyclic oxidation diffraction patterns of the coating deposited on 316L steel from 5 to 50 cycles (a) and from 100 to 300 cycles (b). There is evidence of the appearance of corrosion products such as $ZrO_2$, TiO, $Fe_2O_3$, CrO, and $SiO_2$, with identification PDF00-049-1642, PDF01-077-

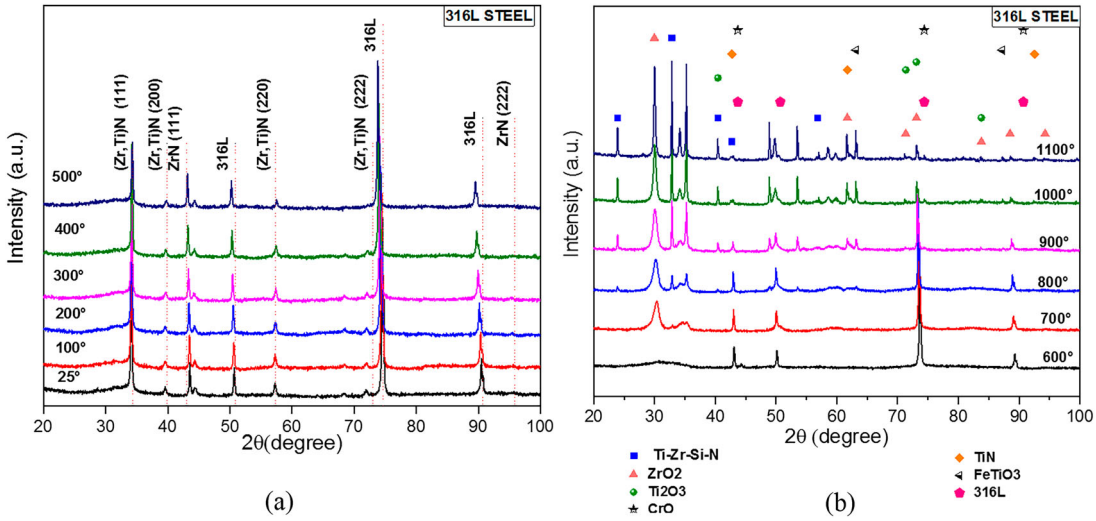


**Figure 5.** XRD patterns of Ti-Zr-Si-N coating with substrate heated up to 1100°C, with temperature variation every 100°C.

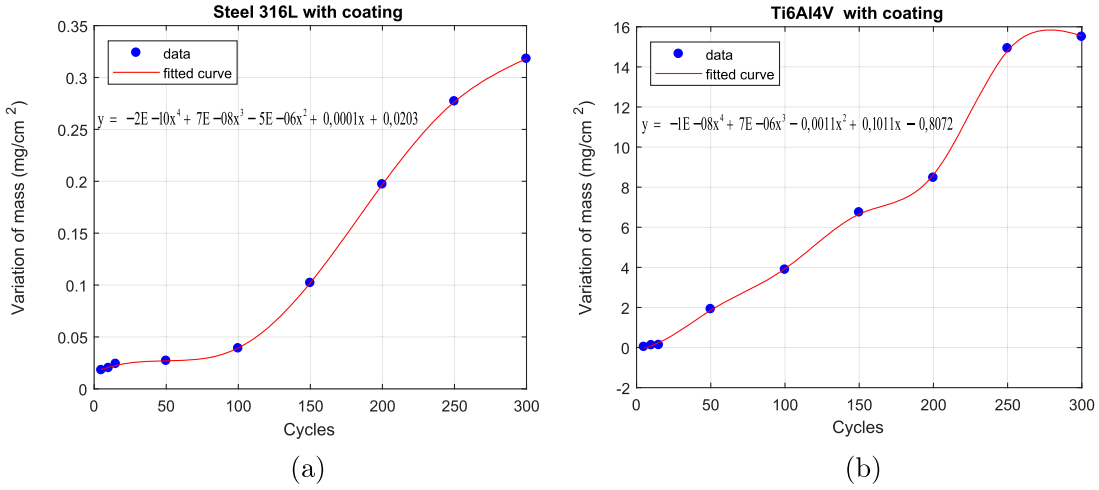


**Figure 6.** Results of mass variation during 300 thermal cycles for the Ti-Zr-Si-N coating deposited on (a) 316L steel and (b) Ti6Al4V alloy.

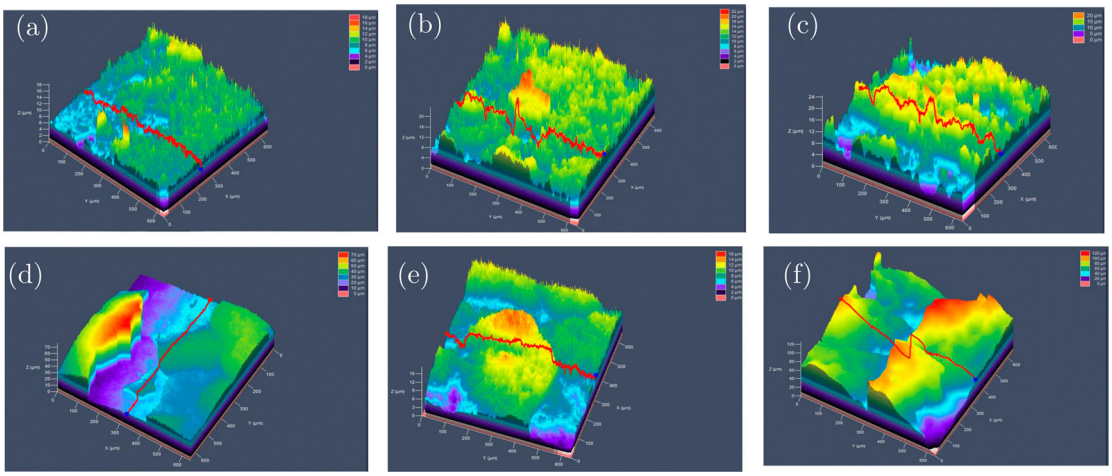


**Figure 7** . Behaviour of the coating subjected to oxidation on 316L steel substrate (a) 100 cycles, (b) 200 cycles, (c) 300 cycles, and on Ti6Al4V substrate (d) 100 cycles, (e) 200 cycles, (f) 300 cycles.

2170, PDF01-073-0603, and $SiO_2$ PDF01-081-0069, respectively, for the coating-substrate system of 316L steel. These oxides that are formed match those observed by Pogrebnjak et al. [22], with an XRD pattern taken for the Ti-Zr-Si-N coating after being subjected to annealing at a temperature of 800° C, where $TiO_2$, $ZrO_2$, TiO, $Fe_2O_3$, and TiN are found. The formation of chromite is also possible, by the reaction of the chromium of stainless steel with air [23], which has been observed in oxidation processes from the grain boundaries to the centre.

Rebouta et al. [24] indicated in their study that (TiZr) N exhibits an oxidation rate at 500° C that is higher than the oxidation rate of other compounds such as (TiAl) N. The presence of zirconium does not significantly change the

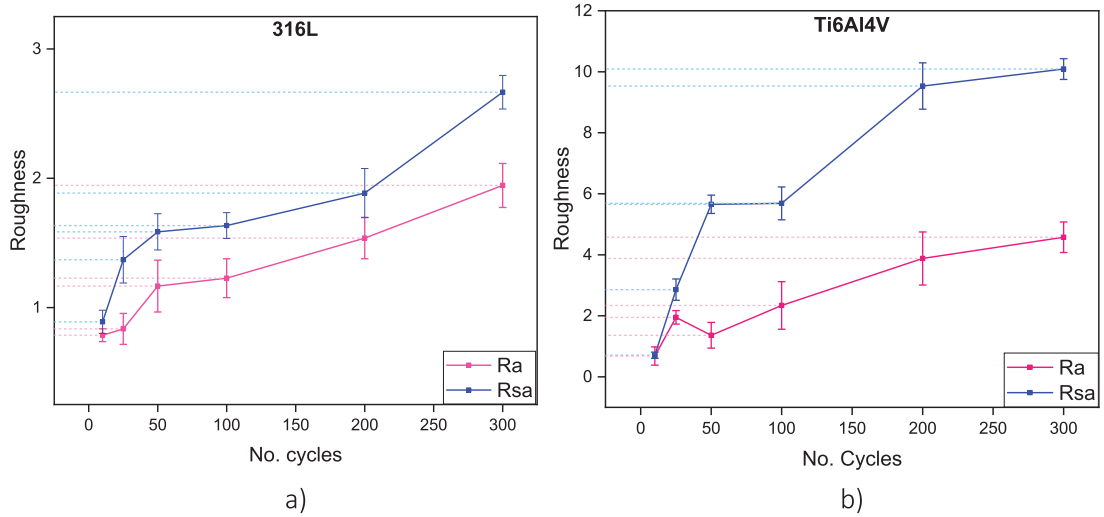


**Figure 8.** Roughness for coating deposited on (a) 316L steel and (b) Ti6Al4V alloy.

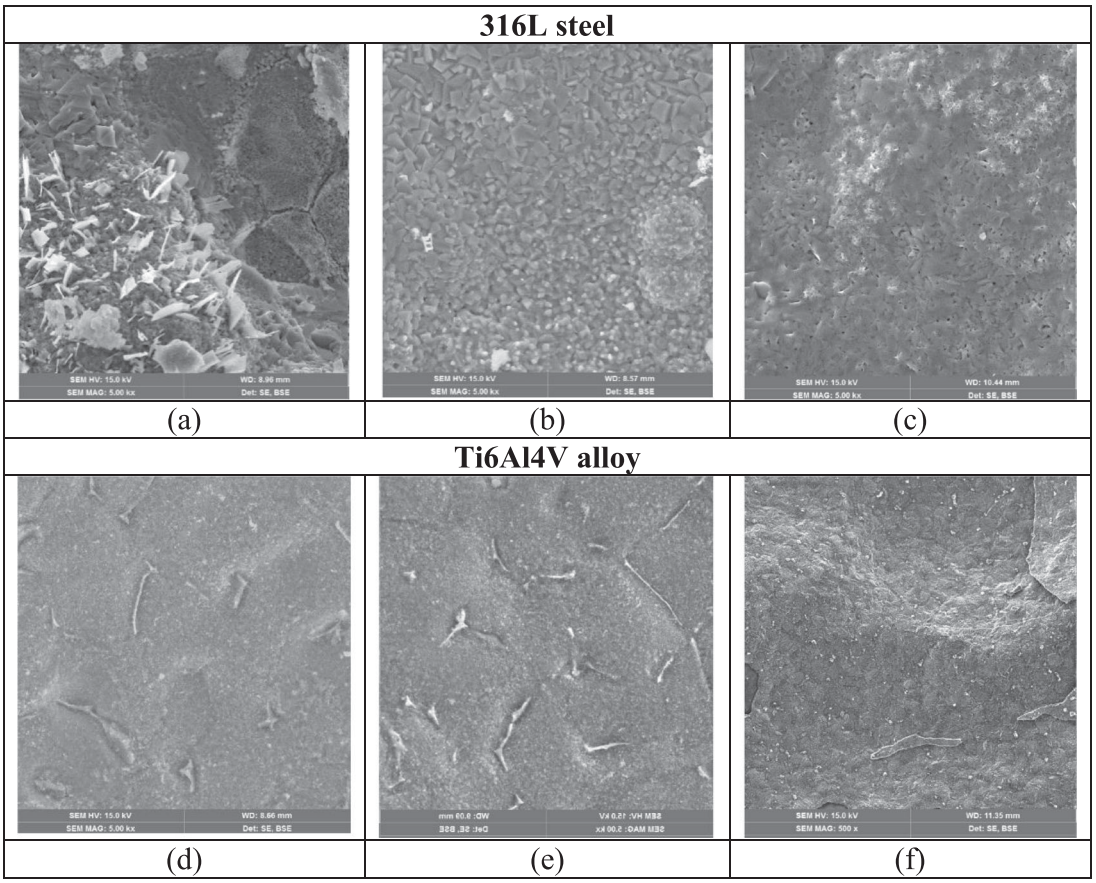


**Figure 9.** SEM analysis for the coating subjected to oxidation on 316L steel substrate (a) 100 cycles, (b) 200 cycles, (c) 300 cycles, and onTi6Al4V alloy substrate (d) 100 cycles, (e) 200 cycles, (f) 300 cycles.

oxidation rate in comparison with the oxidation rate of titanium nitride TiN, which could be related to the results obtained in the present investigation with the appearance of TiO. In addition to the deposited coating, the function of the AISI 316L stainless steel substrate stands out for its very stable corrosion potential as environmental conditions are modified [24,27], as in the case of the present study, being thermodynamically stable.

Figure 11 shows the cyclic oxidation diffraction patterns of the coating on the Ti6Al4V alloy from 5 to 50 cycles (a) and from 100 to 300 cycles (b). Peaks of the oxides formed can be seen, such as $SiO_2$, $ZrO_2$, and TiN; the latter disappears in the final cycles. Rutile peaks of medium intensity can be seen at 27.44°, 54.34°, 56.66°, 62.97°, 74.53°, and 89.58°. The produced coating improved the resistance to oxidation due to its nanocomposite structure and also to the formation of a passive layer of silicon dioxide next to the titanium dioxide layer on the surface of this coating [20,28].

The corrosion mechanism of this system is divided into various stages. Initially, at high temperatures, the adsorption of gaseous species occurs, in this case oxygen between the metal-substrate interface, generating micro-vacuums and

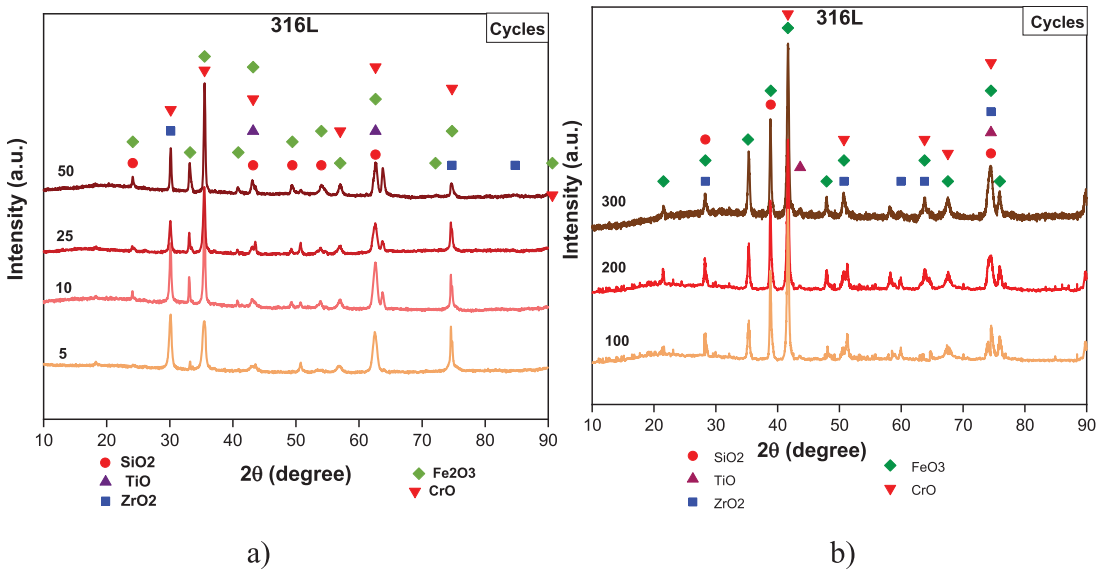


**Figure 10.** Cyclic oxidation diffractogram of the coating on 316L steel substrate (a) up to 50 cycles and (b) up to 300 cycles.

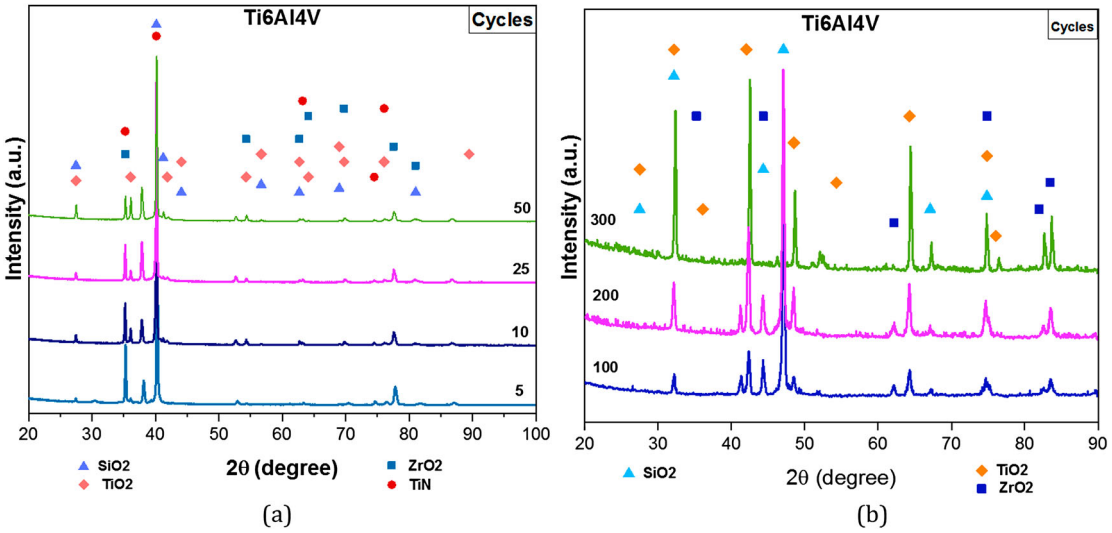


**Figure 11.** Cyclic oxidation diffractogram of the coating on Ti6Al4V alloy substrate (a) up to 50 cycles and (b) up to 300 cycles.

vacancies resulting from the microstructural reorganisation of the coating with micro-vacuums through which the diffusion process between species is activated from the substrate towards the surface, resulting in the generation of non-homogeneous and isolated islands of metal oxides in the substrate-coating interface, which could protect it against degradation. Likewise, a process of microstructural transformation of the coating is activated, producing an evolution from the amorphous to the crystalline phase in the case of coatings with a high percentage of silicon [20]. By increasing the thermal cycles, the diffusion process increases inside the interface, producing anion movement subject to a gradient of electric potential caused by the oxygen and the temperature, which is absorbed and captured by the electrons on the surface of the interface. Furthermore, there is movement of metal cations during the stage of oxide growth towards the outside that generates voids that separate the oxide layer and the substrate.

During the cyclic test, there is growth of crystals with grain formation and an oxide film on the surface, so the oxide nucleation is fully achieved when it comes into immediate contact with oxygen, generating the formation of a very thin rust scale with agglomeration and growth that covers it completely. When a metal reacts with oxygen, it is characterised by the change in free energy that accompanies the formation of its oxide [20,21].

Finally, the presence of thermal stresses during the cyclic test causes the release of protective oxide layers, so that the damage produced in these layers is generated by the increase of thermal stresses during the cooling process. These thermal stresses are caused by the difference in the thermal expansion coefficients between the metal and the oxide layer. This could be relevant for the present investigation, since for the substrates the same thing happened [21].

## Conclusions

Ti-Zr-Si-N coatings deposited on 316L steel exhibited protection against corrosion up to 150 cycles and on Ti6Al4V alloy up to 50 cycles. After this, in the subsequent cycles, a delamination of the coating on the surface of the substrate was observed, exposing it to oxidation.

The deposition of Ti-Zr-Si-N coatings has a favourable effect for the protection of 316L steel against cyclic oxidation at a temperature of 600°, according to the results obtained. The coatings deposited on Ti6Al4V alloy substrates subjected to cyclic oxidation reacted differently from those on 316L steel, where a series of protective layers was formed that increased as a function of the thermal cycles, so based on this evidence, electrolyte transport between the coating surface and the coating-substrate interface through defects such as pores and cracks generated by high-temperature diffusion events can be inferred.

The thermal shock produced by the heating and cooling process due to cyclic oxidation generates stresses, causing the oxide layer to crack and flush, leaving the substrate bare and allowing corrosion of the substrate, as evidenced by the results of the present investigation, since the defects presented are the product of the cyclic oxidation tests.

## Disclosure statement

No potential conflict of interest was reported by the authors.

## Funding

The authors acknowledge the financial support of the Project of the Universidad Nacional de Colombia (UNAL) 'RESISTENCIA A LA CORROSIÓN DE RECUBRIMIENTOS DE (Ag,Zr,Si)N y (Ti,Zr,Si)N PRODUCIDOS POR CO-SPUTTERING REACTIVO'.

## ORCID

*Julieta Cardenas* http://orcid.org/0000-0001-6039-3924
*Jersson Leon* http://orcid.org/0000-0002-9198-1996
*Jhon J. Olaya* http://orcid.org/0000-0002-4130-9675

## References

[1] Kirik GV, Kozak C, Opielak M. Protective coatings based on Zr-Ti-Si-N their physical and mechanical properties and phase composition. Przeglad Elektrotechniczny. 2012;88(10A):319–321.
[2] Pilloud D, Dehlinger AS, Pierson JF, et al. Reactively sputtered zirconium nitride coatings: structural, mechanical, optical and electrical characteristics. Surf Coat Technol. 2003;174:338–344.
[3] Kannan A, Reddy P. The effect of annealing on the structural, optical and electrical properties of titanium nitride (TiN) thin films prepared by DC magnetron sputtering with supported discharge. J Mater Sci: Mater Electron.. 2016; 27 (10):10427–10434.

[4] Leclair P, Berera GP, Moodera JS. Titanium nitride thin films obtained by a modified physical vapor deposition process. Thin Solid Films. 2000;376(1–2):9–15.
[5] Ingason AS, Magnus F, Agustsson JS, et al. In-situ electrical characterization of ultrathin TiN films grown by reactive dc magnetron sputtering on $SiO_2$. Thin Solid Films. 2009;517(24):6731–6736.
[6] Cui X, Jin G, Hao J, et al. The influences of Si content on biocompatibility and corrosion resistance of Zr-Si-N films. Surf Coat Technol. 2013;228:S524–S528.
[7] Kavitha A, Kannan R, Reddy PS, et al. The effect of annealing on the structural, optical and electrical properties of titanium nitride (TiN) thin films prepared by DC magnetron sputtering with supported discharge. J Mater Sci: Mater Electron. 2016;27(10):10427–10434.
[8] Paldey S, Dee SC. Single layer and multilayer wear resistant coatings of (Ti, Al) N: a review. Mater Sci Eng A. 2003;342(1–2):58–79.
[9] Uglov VV, Anishchik VM, Khodasevich VV, et al. Structural characterization and mechanical properties of Ti–Zr–N coatings, deposited by vacuum arc. Surf Coat Technol. 2004;180:519–525.
[10] Chinsakolthanakorn S, Buranawong A, Witit-anun N. Characterization of nanostructured TiZrN thin films deposited by reactive DC magnetron co-sputtering. Procedia Eng. 2012;32:571–576.
[11] Lin Y, Huang J, Yu G. Effect of nitrogen flow rate on properties of nanostructured TiZrN thin films produced by radio frequency magnetron sputtering. Thin Solid Films. 2010;518(24):7308–7311.
[12] Jiang N, Shen YG, Mai Y, et al. Nanocomposite Ti–Si–N films deposited by reactive unbalanced magnetron sputtering at room temperature. Mater Sci Eng B. 2004;106(2):163–171.
[13] Hu X, Han Z, Li G, et al. Microstructure and properties of Ti–Si–N nanocomposite films. J Vac Sci Technol A. 2002;20:1921.
[14] Saladukhin IA, Abadias G, Michel A, et al. Structure and hardness of quaternary TiZrSiN thin films deposited by reactive magnetron co-sputtering. Thin Solid Films. 2015;581:25–31.
[15] Sobol' OV, Pogrebnyak AD, Beresnev VM. Effect of the preparation conditions on the phase composition, structure, and mechanical characteristics of vacuum-Arc Zr-Ti-Si-N coatings. Phys Met Metallogr. 2011;112(2):188–195.
[16] Pogrebnyak AD, Sobol' OV, Beresnev VM, et al. Features of the structural state and mechanical properties of ZrN and Zr(Ti)-Si-N coatings obtained by ion-plasma deposition technique. Tech Phys Lett. 2009;35(10):925–928.
[17] Lin YW, Huang JH, Yu GP, et al. Influence of ion bombardment on structure and properties of TiZrN thin film. Appl Surf Sci. 2015;354:155–160. doi:10.1016/j.apsusc.2015.02.190.
[18] Yalamanchili K, Forsén R, Jiménez-Piqué E, et al. Structure, deformation and fracture of arc evaporated Zr-Si-N hard films. Surf Coat Technol. 2014;258:1100–1107.
[19] Braic M, Braic V, Vladescu A, et al. Solid solution or amorphous phase formation in TiZr-based ternary to quinternary multi-principal-element films. Prog Nat Sci. 2014;24(4):305–312.
[20] Borja EN, Olaya JJ. A microstructural and corrosion resistance study of (Zr, Si. Ti)N-Ni coatings produced through co-sputtering. Dyna. 2018;85(207):192–187.
[21] Bolívar-Osorio FJ. Evaluation of the behavior at high temperatures of the coatings of aluminum, Si and aluminum modified with Si and Hf deposited through CVD-FBR on ferriform-martensitic steels (9-12% of Cr)[dissertation]. Madrid (Spain): Universidad Complutense de Madrid; 2009.Spanish.
[22] Pogrebnjak AD, Shpak AP, Beresnev VM, et al. Effect of thermal annealing in vacuum and in air on nanograin sizes in hard and superhard coatings Zr–Ti–Si–N. J Nanosci Nanotechnol. 2012;12(12):9213–9219.
[23] Marulanda-Arevalo JL, Remolina-Millan A, Baron JA. Steam oxidation in stainless steel AISI 317 at 700 and 750° C. Dyna. 2013;80(179):151–156.
[24] Rebouta L, Vaz F, Andritschky M, et al. Oxidation resistance of (Ti,Al,Zr,Si)N coatings in air. Surf Coat Technol. 1995;76:70–74.
[25] Beresnev VM, Klimenko SA, Toryanik IN, et al. Superhard coatings of the (Zr-Ti-Si)N and (Ti-Hf-Si)N systems produced by vacuum-arc deposition from a separated flow. J Superhard Mater. 2014;36(1):29–34.
[26] Pogrebnjak A, Baidak V, Beresnev V, et al. Physical-mechanical properties of superhard nanocomposite coatings on base Zr-Ti-Si-N. Mater Sci. 2013;19(2):140–143.
[27] Kumar PA, Pandey S, Mishra R, et al. Characterization of stainless steel 316 l coated by thermal spray coating. Int J Adv Res Ideas Innov Technol. 2016;2(3):1–7.
[28] Zhang S, Sun D, Bui XL. Nanocomposite thin films and coatings processing, properties and performance. London: Imperial College Press; 2002; Chapter 1, Magnetron sputtered hard and yet tough nanocomposite coatings with case studies: nanocrystalline TiN embedded in amorphous SiNx; p. 1–110.